Journal of Power Sources 226 (2013) 1–7

Contents lists available at SciVerse ScienceDirect

Journal of Power Sources

journal homepage: www.elsevier.com/locate/jpowsour

Comparative characterization of thermodynamic, electrical, and electrochemical properties of $Sm_{0.5}Sr_{0.5}Co_{1-x}Nb_xO_{3-\delta}$ ($x = 0$, 0.05, and 0.1) as cathode materials in intermediate temperature solid oxide fuel cells

Seonyoung Yoo [a], Tak-Hyoung Lim [b], Jeeyoung Shin [c], Guntae Kim [a,*]

[a] Interdisciplinary School of Green Energy, Ulsan National Institute of Science and Technology (UNIST), Ulsan 689-798, Republic of Korea
[b] Hydrogen & Fuel Cell Department, Korea Institute of Energy Research (KIER), Daejeon 305-343, Republic of Korea
[c] Department of Mechanical Engineering, Dong-Eui University, Busan 614-714, Republic of Korea

HIGHLIGHTS

- $Sm_{0.5}Sr_{0.5}Co_{1-x}Nb_xO_{3-\delta}$ ($x = 0$, 0.05, and 0.1) are investigated by the effect of Nb.
- Electrical properties are identified by a four-terminal d.c. arrangement in air.
- Electrochemical performances are investigated using an Ni–GDC anode-supported cell.
- Thermodynamic properties are estimated from the oxygen isotherms.

ARTICLE INFO

Article history:
Received 23 August 2012
Received in revised form
13 October 2012
Accepted 15 October 2012
Available online 29 October 2012

Keywords:
Solid oxide fuel cells
Perovskite
Coulometric titration
Thermodynamic property
Electrochemical performance

ABSTRACT

The perovskite oxides, such as $(La,Sr)CoO_3$ and $(Ba,Sr)CoO_3$, have received much attention in recent years as cathode materials for intermediate temperature solid oxide fuel cells (IT-SOFCs). In this study, we have investigated the structural, electrical, electrochemical, and redox properties of $Sm_{0.5}Sr_{0.5}Co_{1-x}Nb_xO_{3-\delta}$ (SSCNbx) cathodes under conditions relevant to IT-SOFC operation. The SSCNbx ($x = 0$, 0.05, and 0.1) oxides show gradually decreasing electrical conductivity with increasing Nb doping at the same temperature. The maximum power density of SSCNbx ($x = 0.05$, 0.1) is lower than that of SSC; however, SSCNbx ($x = 0.1$) is more stable than SSC considering the thermodynamic behaviour, as determined through redox isotherms. These results suggest that an Nb doped SSC perovskite is suitable, considering its high power density and reasonable redox stability, as an IT-SOFC cathode material.

1. Introduction

Solid oxide fuel cells (SOFCs) have been studied as a new power generation device on the strengths of their high conversion efficiency, low emissions, and excellent fuel flexibility. The requirement for high operating temperature ranging from 800 to 1000 °C, however, raises crucial issues such as high material costs and high rates of formation of electrical and chemical insulating phases during the cell fabrication and operation. The focus of recent research on SOFC technology has thus shifted towards intermediate temperature operation ranging from 500 to 700 °C [1–3]. The reduction of operating temperature, however, leads to a significant decrease in cathode activity. Therefore, an appropriate cathode material for IT-SOFCs should have high electrical conductivities and high catalytic activity for the oxygen reduction reaction as well as a thermal expansion coefficient that is compatible with the electrolyte [4–6].

In this regard, mixed ionic and electronic conductors (MIECs) containing Mn, Fe, Co, and/or Ni with the capability to conduct oxygen ions and electrons simultaneously are strong candidates as IT-SOFC cathodes [7–12]. Among the various MIEC oxides, cobalt containing perovskite oxides such as $(La,Sr)CoO_3$ and $(Ba,Sr)CoO_3$ have attracted strong interest due to their high electrocatalytic activity for the oxygen reduction reaction [13–15]. The high catalytic activity of LSC can be explained by its high ionic conductivity with lower overpotential and high oxygen vacancy concentration, which facilitates rapid migration of oxygen species through the bulk as well as the surface of the electrode material. In addition,

* Corresponding author. Tel.: +82 52 217 2917; fax: +82 52 217 2909.
E-mail address: gtkim@unist.ac.kr (G. Kim).

0378-7753/$ – see front matter © 2012 Elsevier B.V. All rights reserved.
http://dx.doi.org/10.1016/j.jpowsour.2012.10.069

recent reports investigating Co-based perovskites, such as $Sm_{0.5}Sr_{0.5}CoO_{3-\delta}$ (SSC), have also garnered notable attention. Fukunaga et al. measured the reaction of a dense SSC cathode and found that the surface exchange constants are one order of magnitude larger than the corresponding values for $La_{0.6}Sr_{0.4}CoO_{3-\delta}$ [4,14–17].

Co-based perovskites, on the other hand, show very large thermal expansion coefficients (TECs), which causes mismatch between the cathode and electrolyte. This mismatch degrades the long-term stability and durability for thermal cycling in SOFC systems [18–22].

Nagai et al. demonstrated that the stability of the perovskite structure is enhanced by substituting B-sites with cations having a higher valence, and Nb is the most effective dopant for improving the chemical stability of Co-based perovskite oxides [23,24]. It has been reported that the introduction of Nb in the B-sites of cobalt-based perovskites can improve the electrochemical performance and chemical stability for SOFC application, with 10% Nb doping on $BaCo_{1-x}Fe_xO_{3-\delta}$ [25].

Based on these results, Nb doped SSC is regarded as a suitable cathode material that can provide high cell performance and stability. The aim of this study is to assess the behaviour of Nb doped SSC through characterization of the redox properties and electrochemical performances in terms of its application as a cathode for IT-SOFCs.

2. Experimental

$Sm_{0.5}Sr_{0.5}Co_{1-x}Nb_xO_{3-\delta}$ (SSCNb*x*) oxides were synthesized using the Pechini process to form submicron powder particles. Metal nitrates were employed both as metal precursors and oxidizing agents. Citric acid and niobium oxalate hydrate (Alfa aesar, $C_{10}H_5NbO_2 \cdot xH_2O$) were added to a hydrogen peroxide (H_2O_2) solution under heating (~50 °C) to increase the solubility of the Nb-complex. Stoichiometric amounts of $Sm(NO_3)_3 \cdot 6H_2O$ (Aldrich, 99.9%, metal basis), $Sr(NO_3)_2$ (Aldrich, 99+%), and $Co(NO_3)_2 \cdot 6H_2O$ (Aldrich, 98+%) were added into a beaker containing a suitable amount of concentrated nitric acid solution under continuous heating and stirring with the Nb precursor. An adequate amount of ethylene glycol was added into the beaker after the mixture was dissolved. After a viscous resin was formed, the mixture was heated to roughly 300 °C. The resultant powder was pre-calcined at 700 °C for 4 h, and ball-milled in acetone for 24 h. The powder was pressed into pellets and sintered at 1150–1200 °C for 4 h in air. For the measurement of cell performances of SSCNb*x* cathodes, slurries consisting of powders, GDC, and an organic binder at a weight ratio of 6:4:12 were used.

The structure and the morphology of the SSCNb*x* were characterized by X-ray diffraction (XRD) and scanning electron microscopy (SEM). X-ray powder diffraction measurements (Rigaku diffractometer, Cu Ka radiation) were performed to confirm the structure with a scan rate of $0.6^\circ min^{-1}$.

Symmetrical electrochemical cells with a configuration of electrode/GDC/electrode were applied for the impedance studies. $Ce_{0.9}Gd_{0.1}O_{1.95}$ (GDC) was used for the electrolyte to avoid interfacial reactions between the electrolyte and the cathode, because the LSGM electrolyte and YSZ electrolyte may react with the Sr doped lanthanide cobaltites [26]. The GDC powder was pressed into pellets, and sintered at 1350 °C for 4 h in air to obtain a dense electrolyte substrate. The cathode slurry was painted onto both surfaces of the dense GDC electrolyte symmetrically and subsequently sintered at 950 °C for 4 h under an air atmosphere.

Electrochemical performances of the SSCNb*x* cathode were evaluated with Ni–GDC anode-supported single cells. To measure cell performance, the SSCNb*x* powders and GDC were mixed at a weight ratio of 6:4 and ball-milled for 12 h. The Ni–GDC cermet anode, thereafter, was fabricated from a mixture of nickel oxide, GDC prepared by GNP, and starch at a weight ratio of 6:4:1.5. This mixture was ball-milled in ethanol for 24 h. The GDC powder electrolyte was pressed over the pelletized Ni–GDC cermet anode. The Ni–GDC/GDC anode–electrolyte layer was sintered at 1350 °C for 5 h. For the top layer cathode, the SSCNb slurries were painted on the GDC electrolyte. The cells, with an active electrode area of 0.36 cm^2, were finally sintered at 950 °C for 4 h under an air atmosphere. Ag wires were attached to both the anode and cathode of a single cell using Ag paste (SPI Supplies, 05063-AB) as a current collector. An alumina tube was employed to fix the single cell using a ceramic adhesive (Aremco, Ceramabond 553). H_2 containing 3% H_2O was applied through a water bubbler with a flow rate of 20 mL min^{-1}, while air was applied as an oxidant and supplied to the cathode by ambient air flow during the single cell test. A Bio-Logic Potentiostat was used to measure impedance spectra and *I–V* curves. Impedance spectra were recorded under OCV in a frequency range of 1 mHz–500 kHz with AC perturbation of 14 mA at 700 °C. *I–V* polarization curves were measured between 500 and 650 °C.

Coulometric titration was used to evaluate the exact redox state of a composite as a function of $p(O_2)$. The detailed procedure has been described elsewhere [27]. The oxide-sample was placed in a sealed container at the temperature of interest and equilibrated sufficiently by passing a mixture of gases (5% O_2 in Ar) over it. The yttria-stabilized zirconia (YSZ) tube (McDanel Advanced Ceramic Technologies, Z15410630) was used both to electrochemically pump oxygen out of the system and to sense the equilibrium $p(O_2)$ inside the tube. The criterion we used for establishing equilibrium in coulometric titration was that the potential of the oxygen sensor changed by less than 1 mV h^{-1}. The electrical conductivity of the composite slabs was measured via the 4-probe method with a BioLogic Potentiostat.

3. Results and discussion

Fig. 1(a) presents typical XRD patterns of SSC fired at 1150 °C and SSCNb*x* ($x = 0.05$, 0.1, 0.15, and 0.2) fired at 1200 °C. The patterns suggest that the SSCNb*x* samples have a single-phase perovskite structure without any detectable impurity phases up to $x = 0.1$ and the $Sr(Co_{0.5}Nb_{0.5})O_3$ secondary phase (JCPDS 00-052-0666) started to form with Nb content above $x = 0.1$. This indicates that SSC can form a solid-solution with Nb content of $x \leq 0.1$.

The XRD powder pattern of the SSCNb*x* cathode is analyzed by Rietveld refinement to demonstrate its crystal structure. The SSCNb*x* ($x = 0.1$) cathode could be indexed to an orthorhombic structure (space group: *Pbnm*), as illustrated in Fig. 1(b). As summarized in Table 1, the unit cell parameters increase with increasing Nb content, leading to an increase of unit cell volume. While the valence states of Co ions mostly are +3 or +4, Nb ions exist as a fixed valence state of +5 in SSCNb*x* oxides. If Nb^{5+} ions are substituted for Co^{3+} or Co^{4+} in B-sites, a reduction of Co ions (from Co^{4+} to Co^{3+}) and/or a decrease of oxygen vacancy concentration would occur to maintain electroneutrality [28,29].

XRD patterns of SSCNb*x*–GDC powder composites calcined at 1000 °C are obtained in order to check their chemical stability. There appear to be no detectable reactions between SSCNb*x* and GDC and the patterns verify that the SSCNb*x* ($x = 0.1$) sample, for example, maintains a stable perovskite structure, as seen in Fig. 2.

Cross-sectional SEM images of a single cell and cathode are displayed in Fig. 3. The bottom side indicates the microstructure of the dense GDC electrolyte and the upper side shows the microstructure of the porous cathode made of SSCNb*x*–GDC ($x = 0.1$) after calcination at 950 °C, as presented in Fig. 3(a). The thickness of

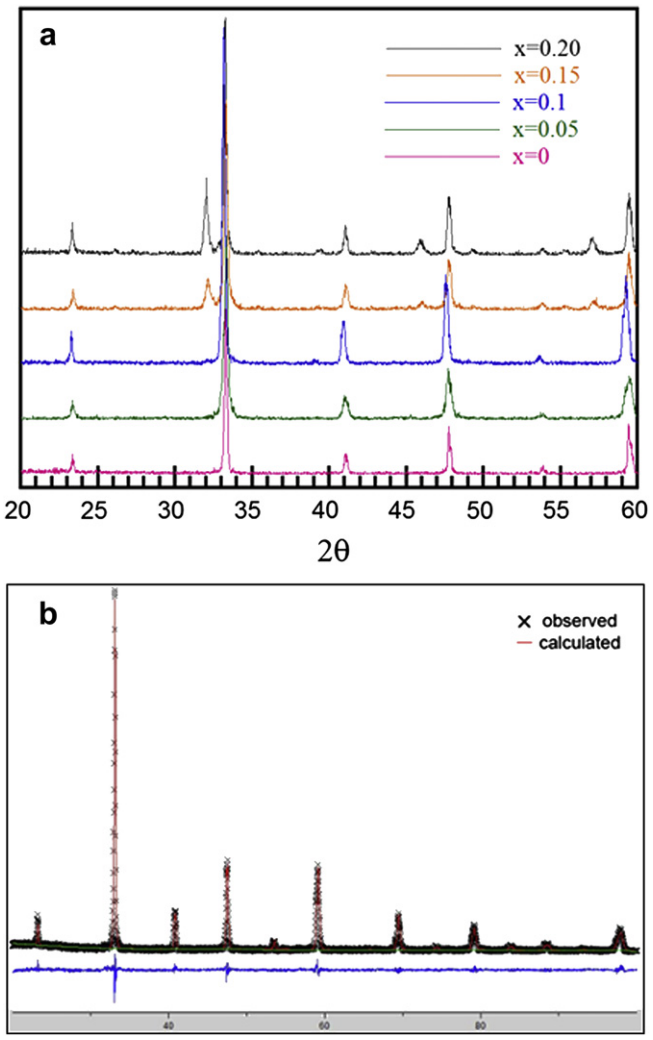

Fig. 1. (a) XRD pattern of $Sm_{0.5}Sr_{0.5}Co_{1-x}Nb_xO_{3-\delta}$ after sintered at 1150–1200 °C, and (b) Rietveld refinement of $Sm_{0.5}Sr_{0.5}Co_{1-x}Nb_xO_{3-\delta}$ ($x = 0.1$) data from room temperature.

the cathode layer and the GDC electrolyte is approximately 15–20 μm, respectively. The microstructure of all SSCNb*x* ($x = 0$, 0.05, and 0.1) samples is similar, thus showing that the microstructures of the samples are apparently insensitive to Nb substitution.

The thermogravimetric analysis of SSCNb*x* cathodes with temperature in air is shown in Fig. 4. The room temperature oxygen content of SSCNb*x* ($x = 0$, 0.05, and 0.1) is set to be 3.0 through iodometric titration. The TGA curves show that significant weight loss occurs above 300 °C due to the loss of oxygen from the lattice. The weight loss of the sample over the entire temperature range decreases with increasing Nb content, possibly due to the stronger Nb–O bond compared to the Co–O bond, which would suppress the oxygen loss of the samples with high Nb content upon heating the samples.

Table 1
Space group and structure parameters of $Sm_{0.5}Sr_{0.5}Co_{1-x}Nb_xO_{3-\delta}$ oxides.

x	Space group	a (Å)	b (Å)	c (Å)	Volume (Å)^3	Oxygen contents
0	*Pbnm*	5.3979	5.3883	7.6243	221.7566	3.0
0.05	*Pbnm*	5.4294	5.3923	7.6216	223.1372	3.0
0.1	*Pbnm*	5.4333	5.4037	7.6400	224.3098	3.0

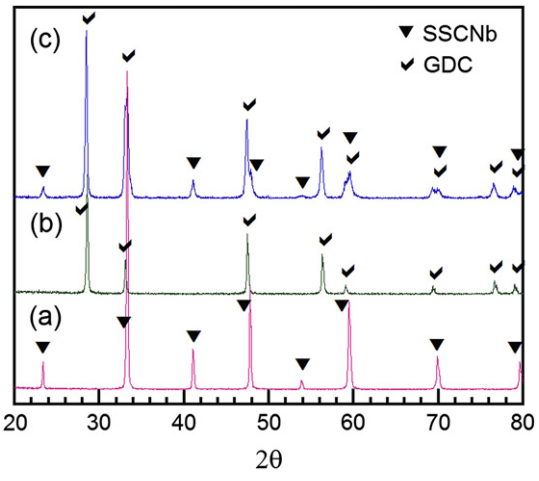

Fig. 2. XRD patterns for (a) $Sm_{0.5}Sr_{0.5}Co_{0.9}Nb_{0.1}O_{3-\delta}$ powder, (b) GDC electrolyte, (c) $Sm_{0.5}Sr_{0.5}Co_{0.9}Nb_{0.1}O_{3-\delta}$–GDC composite after sintered at 950 °C for 4 h.

The temperature dependence of the electrical conductivity of SSC in air is presented in Fig. 5. The electrical conductivity decreased monotonically with temperature, showing metallic behaviour over the entire temperature range. The faster decrease in conductivity at higher temperatures could be due to the formation of a significant amount of oxide ion vacancies [1]. The formation of oxide ion vacancies is accompanied by a reduction of Co^{4+} to Co^{3+}, which results in a decrease of the charge carrier concentration and Co–O covalency, respectively [1,13]. The electrical conductivity decreases with further increases of the Nb doping content. For the perovskite MIECs, simultaneous transport of oxygen ions and electronic conduction is achieved in these oxides. The transport of oxygen ions proceeds through hopping of oxygen vacancies, while transport of electrons is along the B^{n+}–O^{2-}–$B^{(n-1)+}$ network due to overlapping between B:3d and O:2p orbitals [30]. The increase of Nb doping leads to an increase of non-conducting Nb–O bonds, which obstructs electronic transport through O–Co–O bonds and, as a result, the electrical conductivity decreases [29,30].

The impedance spectra for the symmetric cells (SSCNb*x*–GDC/GDC/SSCNb*x*–GDC) by AC impedance spectroscopy with various temperatures in air are shown in Fig. 6. In these spectra, the intercepts with the real axis at low frequency designate the total resistance of the cell and the value of high frequency is the ohmic resistance of the cell. The difference between the two values on the real axis indicates the sum of the cathode–electrolyte interface impedance and non-charge processes, including oxygen surface exchange, solid-state diffusion, and gas-phase diffusion, and is identified as the non-ohmic resistance of the cell [11]. The non-ohmic resistance values of SSCNb*x* ($x = 0$, 0.05, and 0.1) symmetrical cells are 0.061 Ω cm^2, 0.081 Ω cm^2, and 0.107 Ω cm^2, respectively at 650 °C. From these data, the apparent activation energies (E_a) of SSCNb*x* ($x = 0$, 0.05, and 0.1) are calculated to be 100.21 kJ mol^{-1}, 99.20 kJ mol^{-1}, and 96.35 kJ mol^{-1}, respectively. The increase of the ASR with an increase of Nb is possibly due to the decreased electrical conductivity and oxygen vacancy concentration [11,31,32].

The performance of the SSCNb*x* cathodes in SOFCs is measured using the GDC electrolyte with humidified H_2 (3% H_2O) as a fuel and static ambient air as an oxidant in a temperature range of 500–650 °C. Fig. 7 shows the *I*–*V* curves and the corresponding power density of the SSCNb*x* cathodes. The open-circuit voltages of the SSCNb*x* cells are typically 0.8 V at 700 °C and increase with decreasing operating temperature. The maximum power densities

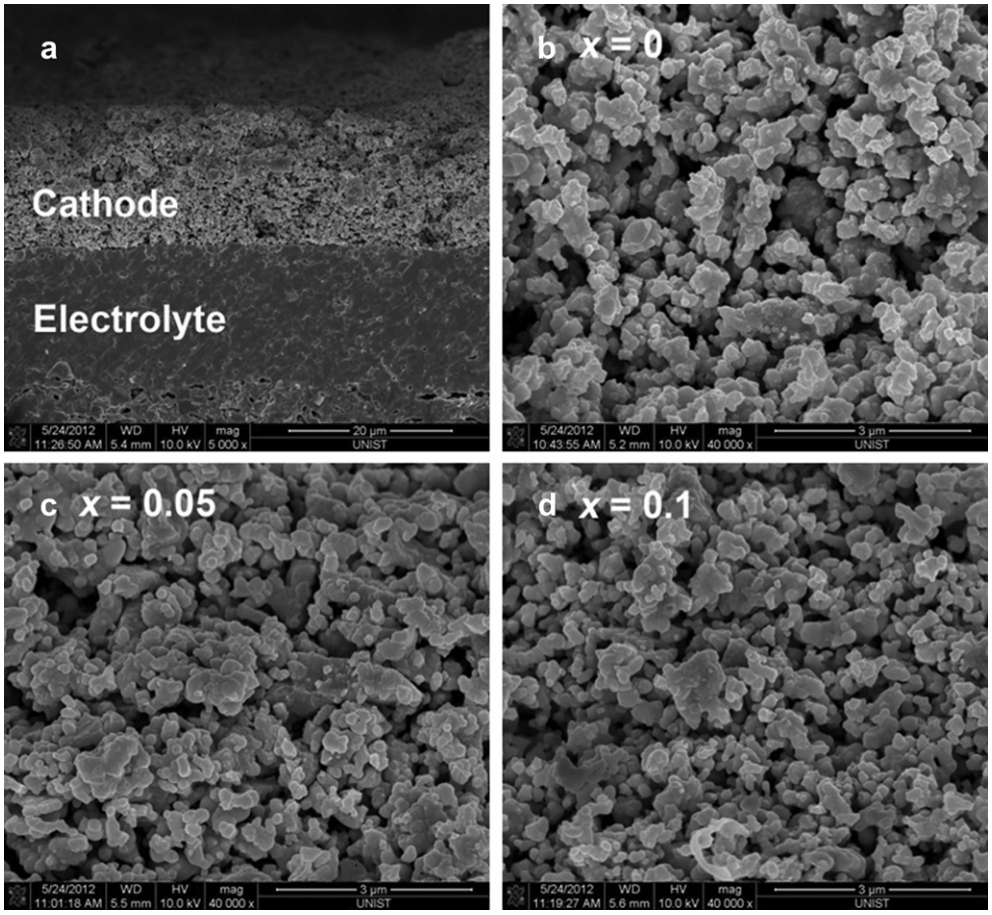

Fig. 3. SEM images of (a) cross-sectional view of the single cell and $Sm_{0.5}Sr_{0.5}Co_{1-x}Nb_xO_{3-\delta}$ cathode with GDC electrolyte in a single cell configuration; (b) $x = 0$, (c) $x = 0.05$, and (d) $x = 0.1$.

of the SSCNbx ($x = 0$, 0.05, and 0.1) cathode material are 1.229, 1.172, and 0.951 W cm^{-2}, at 600 °C, respectively.

The electrical conductivities for SSCNbx measured at various $p(O_2)$ are shown in Fig. 8. The electrical conductivities increased with $p(O_2)$ in all cases over the entire temperature range, indicating that this material is a p-type electronic conductor under the experimental conditions. The predominant defects in SSCNbx are oxygen vacancies, $V_O^{\bullet\bullet}$ and $Co_{Co}^{\bullet}$. The pseudo-chemical reaction between the oxygen vacancies and the surrounding gas can be expressed as Eq. (1) [17,29].

$$\frac{1}{2}O_2 + V_O^{\bullet\bullet} + 2Co_{Co}^{x} \rightleftarrows O_O^{x} + 2Co_{Co}^{\bullet} \quad (1)$$

Therefore, an increase in oxygen partial pressure would lead to a decrease in the concentration of oxygen vacancies and an increase in the concentration of electronic holes, which would in turn

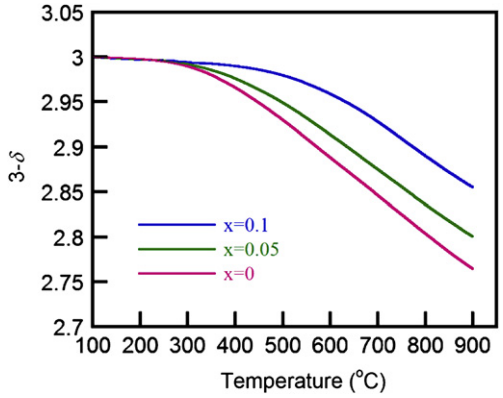

Fig. 4. Thermogravimetric data of $Sm_{0.5}Sr_{0.5}Co_{1-x}Nb_xO_{3-\delta}$ ($x = 0$, 0.05, and 0.1) as a function of temperature.

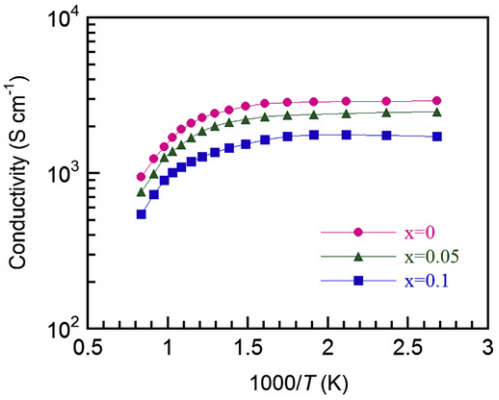

Fig. 5. The electrical conductivity data for $Sm_{0.5}Sr_{0.5}Co_{1-x}Nb_xO_{3-\delta}$ ($x = 0$, 0.05, and 0.1) as a function of temperature in air.

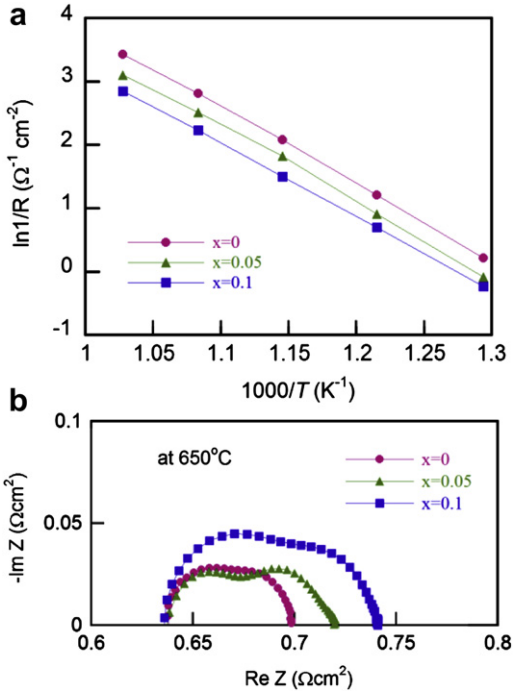

Fig. 6. (a) Arrhenius plot of the area specific resistance for $Sm_{0.5}Sr_{0.5}Co_{1-x}Nb_xO_{3-\delta}$ ($x = 0$, 0.05, and 0.1) at various temperatures.

increase the *p*-type electrical conductivity [11]. The electrical conductivity is high enough at the IT-SOFC operating temperature (650–750 °C) down to a low oxygen partial pressure. The electrical conductivities of SSC dramatically decreased at a $p(O_2)$ of approximately 10^{-6} atm and the SSC appears to decompose thoroughly at a $p(O_2)$ of 10^{-7} atm. In contrast, the electrical conductivities of SSCNb*x* ($x = 0.1$) retain acceptable values down to a lower $p(O_2)$ of 10^{-7} atm. The higher redox stability of SSCNb*x* ($x = 0.1$) than SSC down to a lower $p(O_2)$ at the same temperature is attributed to the positive effect of Nb on the stability [23,24,32].

Fig. 9 shows the equilibrium oxygen nonstoichiometries for SSCNb*x* determined by coulometric titration as a function of $p(O_2)$ at temperatures of 650, 700, and 750 °C [27,33]. Under operation conditions, the interface of SOFCs between the electrolyte and the cathode experiences a lower $p(O_2)$, which may cause redox degradation of the cathode and affect the long-term stability of the cathode performance [34]. The data show that the isotherms of SSCNb*x* at three different temperatures (650, 700, and 750 °C) have similar shapes, suggesting that the reduction mechanisms are quite similar. As the temperature decreases, the decomposition $p(O_2)$ becomes lower and the isotherms are extended to the left and the concentration of oxygen vacancies increases. It is shown that SSCNb*x* ($x = 0.1$) has a higher redox stability than SSC down to a lower $p(O_2)$ at the same temperature. For example, at 700 °C, the SSC sample starts to decay at a $p(O_2)$ of approximately 10^{-6} atm and appears to decompose thoroughly at a $p(O_2)$ of 10^{-7} atm; the SSCNb*x* samples meanwhile are stable to a lower $p(O_2)$, 10^{-7} atm. The higher redox stability of the SSCNb*x* oxides can be a key factor for attaining stable electrochemical properties of a cathode material for viable operation of IT-SOFCs. Therefore, Nb doped SSC oxides can be regarded as suitable cathode materials in terms of redox stability [33].

The partial molar enthalpy and entropy of oxidation can be calculated from the slopes of the isotherms. The Gibbs free energy, ΔG, is related to the equilibrium constant, *K*, and $p(O_2)$ as follows,

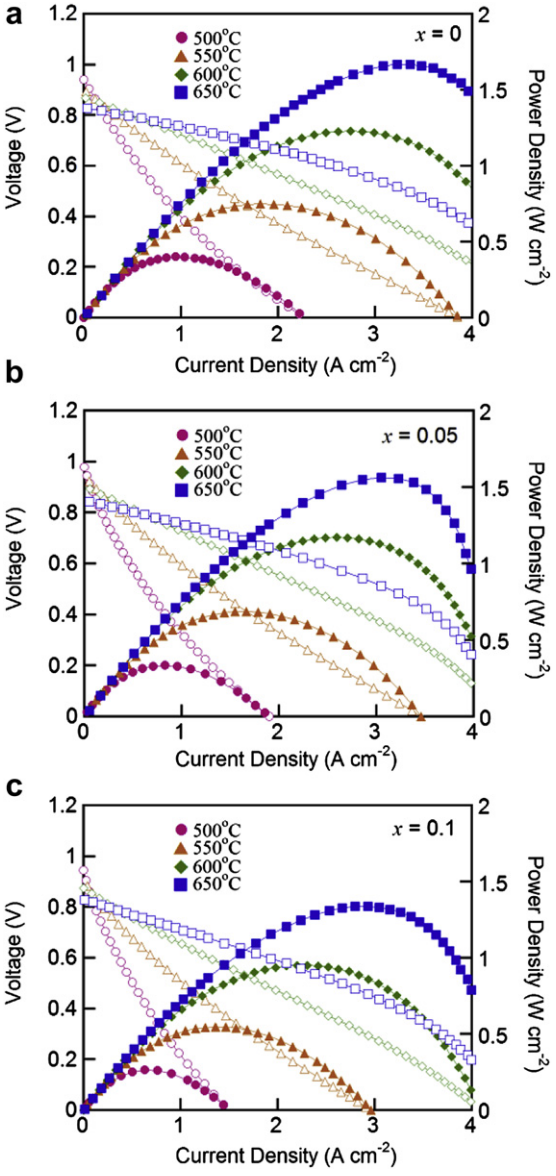

Fig. 7. *I–V* curves and corresponding power density curves of single cell Ni-GDC/GDC/$Sm_{0.5}Sr_{0.5}Co_{1-x}Nb_xO_{3-\delta}$ ($x = 0$, 0.05, and 0.1) in various temperatures.

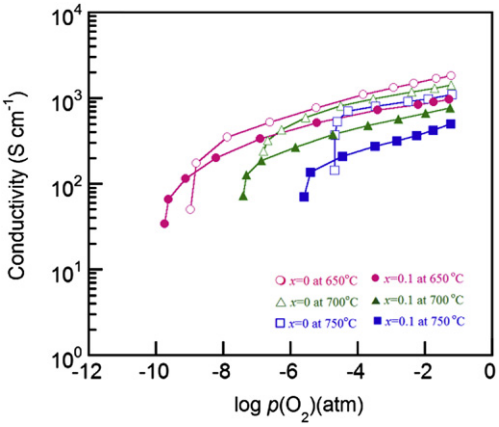

Fig. 8. The electrical conductivities of the $Sm_{0.5}Sr_{0.5}Co_{1-x}Nb_xO_{3-\delta}$ ($x = 0$, 0.1) in various $p(O_2)$.

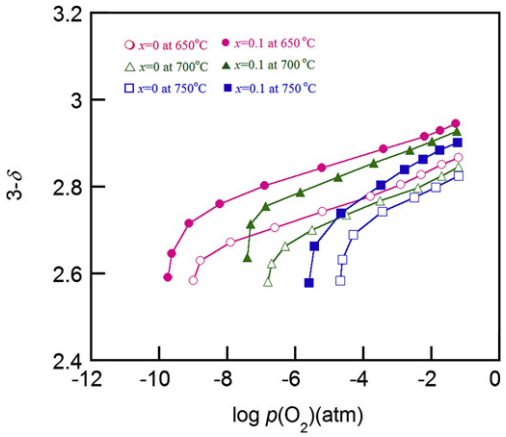

Fig. 9. The isotherms of the $Sm_{0.5}Sr_{0.5}Co_{1-x}Nb_xO_{3-\delta}$ ($x = 0$, 0.1).

$$\Delta G = -RT \ln K = \frac{1}{2} RT \ln p(O_2) \tag{2}$$

At a constant δ, the partial molar enthalpy of oxidation at various temperatures is shown by the Gibbs–Helmholtz equation [35].

$$\Delta H = \frac{\partial\left(\frac{\Delta G}{T}\right)}{\partial\left(\frac{1}{T}\right)} = \frac{R}{2} \frac{\partial \ln [p(O_2)]}{\partial\left(1/T\right)}\Bigg|_{\delta} \tag{3}$$

And the partial molar entropy can be obtained by using the Maxwell relation as follows.

$$-\Delta S = \frac{\partial \Delta G}{\partial T} = \left(\frac{R}{2}\right)\left(\frac{\partial\, T \ln [p(O_2)]}{\partial T}\right)\Bigg|_{\delta} \tag{4}$$

The partial enthalpies of oxidation for SSCNbx are calculated from Eq. (3) and presented in Fig. 10. There are dramatic changes in the oxidation enthalpies according to the extent of reduction. In the case of Nb doped on a Co-based oxide, the energy states of Nb ions are located far above the Fermi level, and thus the electrons released by the formation of oxygen vacancies under a reducing atmosphere would results in little deterioration of the bonds between Nb and O ions. The resilient Nb–O bonding can thus stabilize the oxide. Furthermore, Nb doping raises the formation energy of oxygen vacancies in perovskites [23].

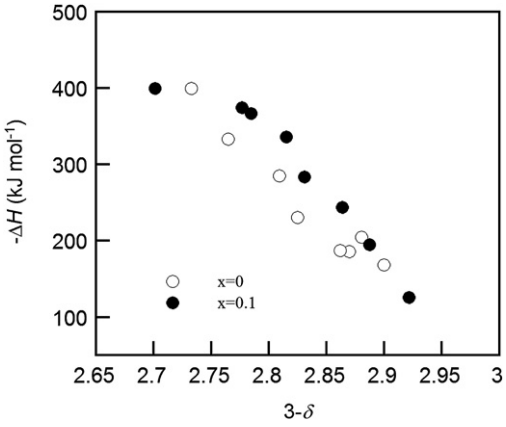

Fig. 10. Partial molar enthalpy of oxidation (ΔH) at 700 °C of $Sm_{0.5}Sr_{0.5}Co_{1-x}Nb_xO_{3-\delta}$ ($x = 0$, 0.1).

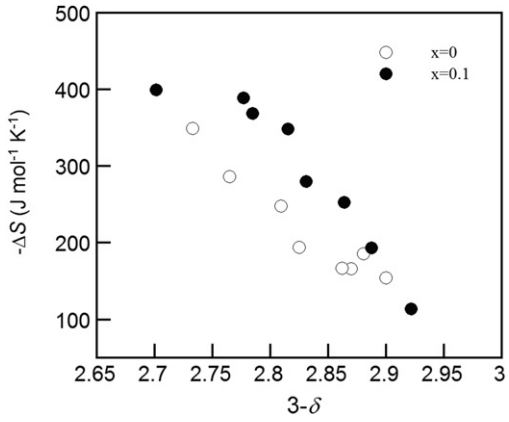

Fig. 11. Partial molar entropy of oxidation (ΔS) at 700 °C of $Sm_{0.5}Sr_{0.5}Co_{1-x}Nb_xO_{3-\delta}$ ($x = 0$, 0.1).

The partial molar entropies of oxidation, calculated from the differences in the Gibbs free energies and the enthalpies, are shown in Fig. 11. It appears that the probability of oxygen vacancy formation rises as the concentration of oxygen vacancies increases.

4. Conclusion

$Sm_{0.5}Sr_{0.5}Co_{1-x}Nb_xO_{3-\delta}$ (SSCNbx) perovskite oxides have been investigated as a cathode material for IT-SOFCs. It is shown that Nb doping has a significant effect on the electrical conductivity, electrochemical performance, and redox stability of the SSCNbx oxides. SSCNbx ($x = 0$, 0.05, and 0.1) oxides show gradually decreasing electrical conductivity with increasing Nb doping at the same temperature. The impedance spectra for symmetric cells are measured by AC impedance spectroscopy at various temperatures in air. The non-ohmic resistance of SSCNbx ($x = 0$, 0.05, and 0.1) symmetrical cells is 0.061 Ωcm^2, 0.081 Ωcm^2, and 0.107 Ωcm^2, respectively, at 650 °C. The increase of the ASR with an increase of Nb is possibly due to the decreased electrical conductivity and oxygen vacancy concentration. The electrochemical performances of SSCNbx are measured using an anode-supported cell based on a GDC electrolyte with humidified H_2 (3% H_2O). The maximum power densities of the single cell are 1.229, 1.172, and 0.951 W cm^{-2}, at 600 °C, respectively, with a SSCNbx ($x = 0$, 0.05, and 0.1)-GDC composite cathode. The maximum power density of SSCNbx ($x = 0.05$, 0.1) is lower than that of SSC; however, SSCNbx ($x = 0.1$) is more stable than SSC considering the thermodynamic behaviour observed from the coulometric titration experiment. From these results, the Nb doped SSC oxide appears to be an acceptable IT-SOFC cathode material, considering its high power density and reasonable redox stability.

Acknowledgements

This research was supported by the Basic Science Research Program (2012R1A1A1013380) and Mid-career Researcher Program (2011-0010773) through the National Research Foundation of Korea, funded by the Ministry of Education, Science and Technology, and a New & Renewable Energy of the Korea Institute of Energy Technology Evaluation and Planning (KETEP) (20113020030060) grant funded by the Korean Ministry of Knowledge Economy.

References

[1] K.T. Lee, A. Manthiram, J. Electrochem. Soc. 153 (2006) A794–A798.

[2] W. Zhou, W. Jin, Z. Zhu, Z. Shao, Int. J. Hydrogen Energy 35 (2010) 1356–1366.
[3] A.J. Jacobson, Chem. Mater. 22 (2010) 660–674.
[4] H. Fukunaga, M. Koyama, N. Takahashi, C. Wen, K. Yamada, Solid State Ionics 132 (2000) 279–285.
[5] W. Zhou, R. Ran, Z. Shao, J. Power Sources 192 (2009) 231–246.
[6] S. Yang, T. He, Q. He, J. Alloys Compd. 450 (2008) 400–404.
[7] E.V. Tsipis, V.V. Kharton, J. Solid State Electrochem. 12 (2008) 1367–1391.
[8] E.P. Murray, M.J. Sever, S.A. Barnett, Solid State Ionics 148 (2002) 27–34.
[9] S. Choi, J. Shin, G. Kim, J. Power Sources 201 (2012) 10–17.
[10] L.M. Acuña, J. Peña-Martínez, D. Marrero-López, R.O. Fuentes, P. Nuñez, D.G. Lamas, J. Power Sources 196 (2011) 9276–9283.
[11] S.B. Adler, J.A. Lane, B.C.H. Steele, J. Electrochem. Soc. 143 (1996) 3554–3564.
[12] S.P. Jiang, Solid State Ionics 146 (2002) 1–22.
[13] S. Park, S. Choi, J. Shin, G. Kim, J. Power Sources 210 (2012) 172–177.
[14] C. Xia, W. Rauch, F. Chen, M. Liu, Solid State Ionics 149 (2002) 11–19.
[15] I.-M. Hung, K.-Z. Fung, C.-T. Lin, M.-H. Hon, J. Power Sources 193 (2009) 116–121.
[16] Y. Guo, D. Chen, H. Shi, R. Ran, Z. Shao, Electrochim. Acta 56 (2011) 2870–2876.
[17] F. Dong, D. Chen, R. Ran, H. Park, C. Kwak, Z. Shao, Int. J. Hydrogen Energy 37 (2012) 4377–4387.
[18] K. Equchi, J. Alloys Compd. 250 (1997) 486–491.
[19] H. Lv, Y. Wu, B. Huang, B. Zhao, K. Hu, Solid State Ionics 177 (2006) 901–906.
[20] S.J. Lee, P. Muralidharan, S.H. Jo, D.K. Kim, Electrochem. Commun. 12 (2010) 808–811.
[21] Y. Zhang, C. Xia, J. Power Sources 195 (2010) 6611–6618.
[22] F. Zhao, R. Peng, C. Xia, Mater. Res. Bull. 43 (2008) 370–376.
[23] P.J. Shen, X. Liu, H.H. Wang, W.Z. Ding, J. Phys. Chem. C 114 (2010) 22338–22345.
[24] T. Nagai, W. Ito, T. Sakon, Solid State Ionics 177 (2007) 3433–3444.
[25] Z. Yang, C. Yang, C. Jin, M. Han, F. Chen, Electrochem. Commun. 13 (2011) 882–885.
[26] L. Dieterle, D. Bach, R. Schneider, H. Störmer, D. Gerthsen, U. Guntow, E. Ivers-Tiffée, A. Weber, C. Peters, H. Yokokawa, J. Mater. Sci. 43 (2008) 3135–3143.
[27] S. Yoo, J.Y. Shin, G. Kim, J. Mater. Chem. 21 (2011) 439–443.
[28] Y. Cheng, H. Zhao, D. Teng, F. Li, X. Lu, W. Ding, J. Memb. Sci. 322 (2008) 484–490.
[29] F. Wang, Q. Zhou, T. He, G. Li, H. Ding, J. Power Sources 195 (2010) 3772–3778.
[30] Z.Q. Deng, W.S. Yang, W. Liu, C.S. Chen, J. Solid State Chem. 179 (2006) 362–369.
[31] Q. Li, H. Zhao, L. Huo, L. Sun, X. Cheng, J.-C. Grenier, Electrochem. Commun. 9 (2007) 1508–1512.
[32] Z.Q. Deng, J.P. Smit, H.J. Niu, G. Evans, M.R. Li, Z.L. Xu, J.B. Claridge, M.J. Rosseinsky, Chem. Mater. 21 (2009) 5154–5162.
[33] S. Yoo, J.Y. Shin, G. Kim, J. Electrochem. Soc. 158 (2011) B632–B638.
[34] D.M. Bastidas, S. Tao, J.T.S. Irvine, J. Mater. Chem. 16 (2006) 1603–1605.
[35] T. Nakamura, K. Yashiro, K. Sato, J. Mizusaki, Solid State Ionics 180 (2009) 368–376.